Neutron scattering study of the magnetic structure of Cs_2CuCl_4

1996 J. Phys.: Condens. Matter 8 7473

(http://iopscience.iop.org/0953-8984/8/40/012)

J. Phys.: Condens. Matter **8** (1996) 7473–7491. Printed in the UK

Neutron scattering study of the magnetic structure of Cs_2CuCl_4

R Coldea†, D A Tennant†, R A Cowley†, D F McMorrow‡, B Dorner§ and Z Tylczynski‖

† Oxford Physics, Clarendon Laboratory, Parks Road, Oxford OX1 3PU, UK
‡ Risø National Laboratory, Department of Solid State Physics, PO Box 49, DK-4000 Roskilde, Denmark
§ Institut Laue–Langevin, BP 156, F-38042 Grenoble Cédex 9, France
‖ Institute of Physics, Umultowska 85, 61-614 Poznan, Poland

Received 2 July 1996

Abstract. The magnetic structure in the ordered phase of the nearly one-dimensional Heisenberg antiferromagnet Cs_2CuCl_4 has been measured using elastic neutron scattering. Cs_2CuCl_4 crystallizes in the orthorhombic *Pnma* space group with Cu^{2+} spin chains running along the crystallographic *b*-direction. Below the ordering temperature $T_N = 0.62 \pm 0.01$ K the magnetic structure is incommensurate along the chain direction with a temperature-independent ordering wavevector $\boldsymbol{q} = (0, 0.472, 0)$ (rlu). The occurrence of an incommensurate structure is shown to be the consequence of frustration on the spins induced by the exchange interaction between chains. Group theory is used to determine the possible magnetic structures compatible with the symmetry of the crystal. The results show that at $T = 0.3$ K the spin ordering is cycloidal with spins rotating in a plane that contains the propagation direction *b*. A mean-field calculation of the magnetic ground-state energy including exchange anisotropy effects is used to study the stability of the observed structure. Values for the interchain exchange constants that are consistent with the features of the magnetic structure are proposed.

1. Introduction

Cs_2CuCl_4 and Cs_2CoCl_4 have been proposed as possible one-dimensional (1D) magnetic materials. Magnetic susceptibility [1] and specific heat measurements [2] have shown that Cs_2CoCl_4 behaves like a nearly 1D $S = \frac{1}{2}$ XY antiferromagnet and a neutron scattering experiment has confirmed the one-dimensional character of the magnetic interactions [3]. The neutron scattering measurements showed diffuse scattering which suggested an incommensurate structure, but the extremely low ordering temperature ($T_N = 0.22$ K) precluded a detailed study of this magnetic structure. Cs_2CuCl_4 has the same crystal structure [4] and very similar lattice parameters. Magnetic susceptibility measurements suggest that it behaves like a nearly 1D $S = \frac{1}{2}$ Heisenberg antiferromagnet with a nearest-neighbour interaction $J = 0.34 \pm 0.01$ meV between spins within the one-dimensional chains and a small antiferromagnetic exchange coupling J' of the order $rJ'/J = 0.050 \pm 0.025$ between the chains, where r is the number of nearest-neighbouring chains [5]. The purpose of this paper is to report on the determination of the magnetic structure of Cs_2CuCl_4 at low temperatures, which gives further information about the magnetic interactions and the ratio of intrachain and interchain exchange interactions.

0953-8984/96/407473+19$19.50

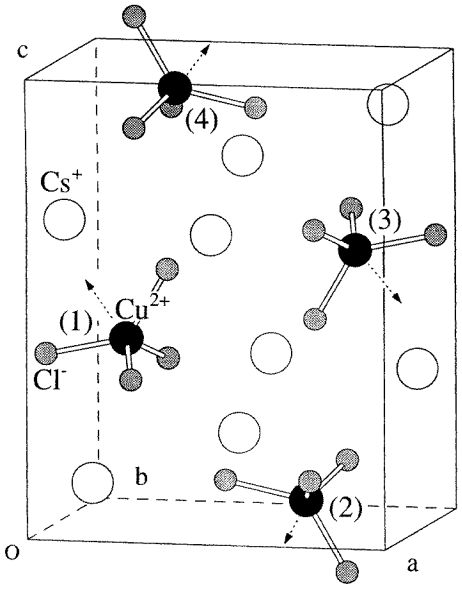

Figure 1. The orthorhombic crystal structure of Cs_2CuCl_4 showing the four independent Cu spins in the unit cell. The local symmetry axis at each Cu site is indicated by a dashed arrow.

Cs_2CuCl_4 has an orthorhombic crystal structure of β-K_2SO_4 type, with space group $Pnma$ (D_{2h}^{16}) [4]. The lattice parameters at 0.3 K are $a = 9.65$ Å, $b = 7.48$ Å and $c = 12.35$ Å. The structure is made up of $CuCl_4^{2-}$ tetrahedra and Cs^+ ions, as shown in figure 1. There are four independent Cu^{2+} ions in the unit cell and they occupy the crystallographic 4c site with the following positions:

$$(1)\colon x, \frac{1}{4}, z$$
$$(2)\colon x + \frac{1}{2}, \frac{1}{4}, -z + \frac{1}{2}$$
$$(3)\colon 1 - x, \frac{3}{4}, 1 - z$$
$$(4)\colon -x + \frac{1}{2}, \frac{3}{4}, z + \frac{1}{2}$$

where $x = 0.23$ and $z = 0.42$ [4]. The predominant exchange interaction is between neighbouring Cu spins along the crystallographic b-direction with the exchange path Cu–Cl–Cl–Cu, so the magnetism is dominated by parallel magnetic chains aligned along the b-axis, as shown schematically in figure 2. There are four independent chains in the unit cell and the Cu atoms in chains (3) and (4) are displaced by $\boldsymbol{b}/2$ with respect to those in chains (1) and (2). The main intrachain exchange interaction J tends to align the Cu spins antiferromagnetically along the chain. The interaction between the chains displaced by $\boldsymbol{b}/2$ introduces an element of frustration, since each spin interacts with two oppositely aligned spins as shown in figure 2. We will show that these competing interactions lead to an incommensurate spin ordering along the chain. A similar situation is encountered in β-MnO_2 where the competing exchange interactions stabilize an incommensurate helimagnetic structure with spins rotating in an easy plane perpendicular to the direction of propagation [6].

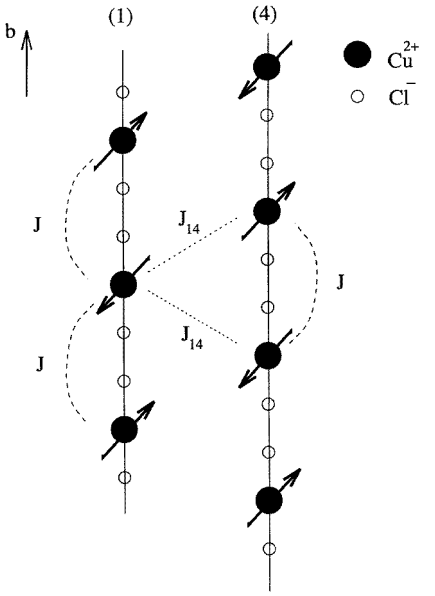

Figure 2. A schematic diagram of chains (1) and (4) which are displaced by ***b***/2 with respect to each other. The arrows on the Cu spins indicate a possible spin ordering in the case when only the exchange interaction J along the chains was present. The exchange interaction J_{14} between the chains induces a frustration on the spins as described in the text.

The outline of the paper is as follows. Section 2 gives details of the experimental arrangement and section 3 presents the results. Section 4 contains both a theoretical analysis of the possible magnetic structures allowed by symmetry and a mean-field calculation of the magnetic ground-state energy. This is followed by analysis and discussion of the results in section 5. The conclusions of the paper are summarized in section 6.

2. Experimental details

The sample used in the neutron scattering experiments was a large single crystal of Cs_2CuCl_4 ($1 \times 1 \times 0.5$ cm^3 in volume), which was reddish-brown in colour and whose mosaic spread was measured to be $9'$. The crystal was grown from aqueous solution with double excess of CsCl at a constant temperature of 310 K, as described in [7].

Susceptibility measurements by Carlin *et al* [5] have suggested that the magnetic ordering temperature of Cs_2CuCl_4 is below 1 K. To achieve these low temperatures in our experiments two different cooling systems were used. The first system was a sorption-pumped ^{3}He fridge that provided a variable-temperature control at the sample position in the range 0.3–300 K with an accuracy at the lowest temperatures of ± 0.005 K and very good stability. The second cooling system used was a dilution fridge insert working inside an ILL variable-temperature cryostat. In this case the temperature range available was 0.1–300 K but with an accuracy of only ± 0.02 K at low temperatures. The sample was aligned with the *a*- and *b*-axes in the scattering plane, where *b* is the direction of the magnetic chains.

The neutron scattering measurements were performed using the TAS7 three-axis crystal spectrometer at the Risø National Laboratory, Denmark and the IN14 three-axis crystal

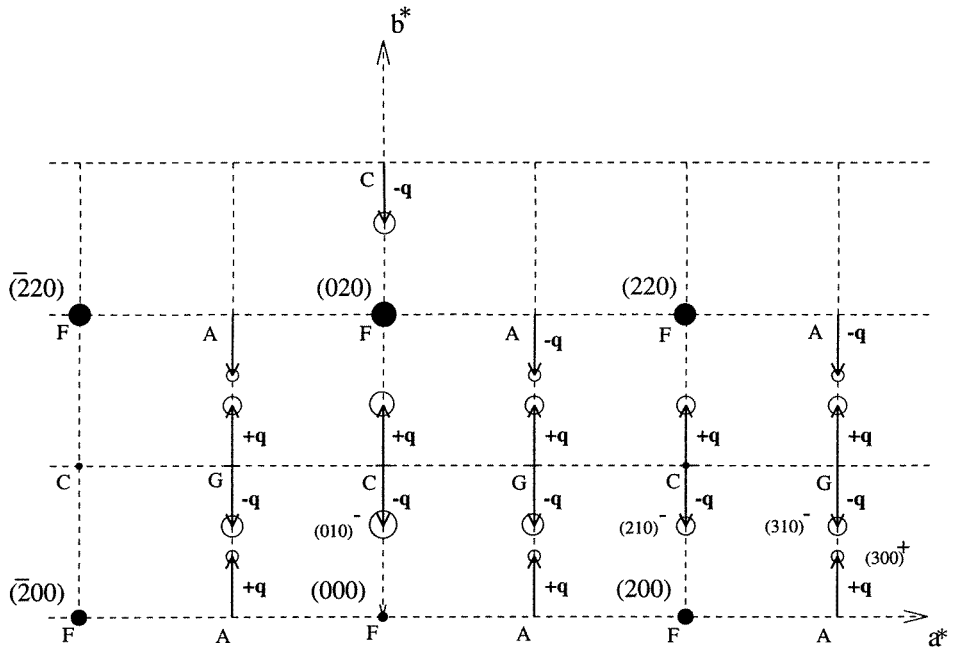

Figure 3. A schematic diagram of the (a, b) scattering plane showing the measured nuclear (filled circles) and magnetic reflections (open circles), where the size of the circles represents the intensity. The magnetic peaks occur at satellite positions around reciprocal-lattice points, as described in the text. The labels F, C, G and A show the extinction rules associated with the four different spin structures allowed by symmetry, as described in section 4.1.

spectrometer at the Institut Laue–Langevin, Grenoble, France. Both spectrometers have cold sources to provide the incident neutrons. A variable-curvature pyrolytic graphite (PG)(002) monochromator was used in the incident neutron beam and the energy of the scattered beam was analysed using the (002) reflection from a flat PG crystal. The spectrometers were used to study the elastic scattering with an incident neutron energy of 5 meV. A cooled Be filter was used before the sample to eliminate the higher-order neutrons. The collimations were chosen to be 28′–OPEN–60′–OPEN (TAS7) and OPEN (40′)–40′–40′–40′ (IN14). The low-temperature magnetic structure was determined from the elastic scattering measured when scanning the wavevector transfer through the magnetic Bragg reflections in reciprocal space along the [100] and [010] directions, and transverse and longitudinal with respect to the scattering wavevector (ω and (θ, 2θ) scans). From the integrated intensities of these reflections, the magnetic structure factors squared were obtained by correcting for the resolution effects [8], the sample mosaic spread [9] and the magnetic form factor of the Cu^{2+} ions [10].

3. Measurements and results

The intensity of the elastically scattered neutrons was measured for the wavevector transfer varying in reciprocal space along $[H, \xi, 0]$ directions with H an integer, where throughout this paper we shall refer to all wavevector transfers in terms of reciprocal-lattice units of the crystallographic structure. At $T = 0.3$ K well defined peaks were observed for ξ close

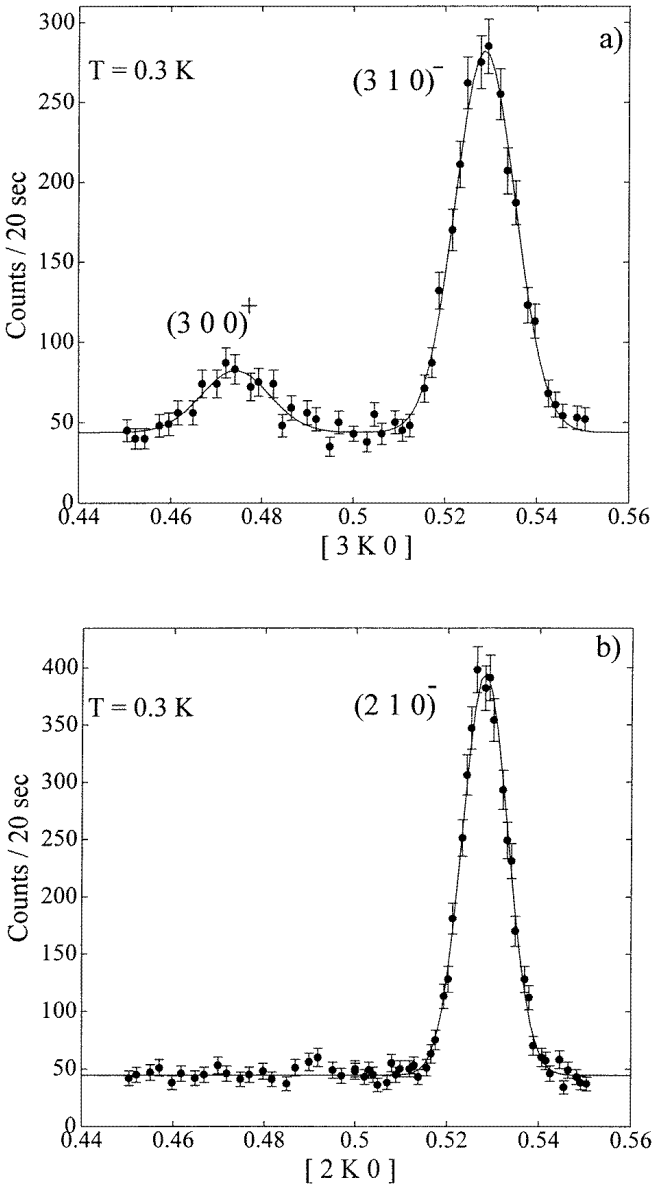

Figure 4. Two sample scans along the chain direction showing the magnetic peaks at $T = 0.3$ K. The solid lines are fits to Gaussians.

to half-odd-integer values, as shown schematically in figure 3. These peaks are magnetic in origin and could not be observed at temperatures above $T_N = 0.62$ K. A characteristic feature of the magnetic reflections is that their position in ξ is not exactly at the half-odd-integer values expected for antiferromagnetic ordering, but displaced. For H even, strong peaks were observed with a displacement that alternated with increasing ξ and an intensity that decreased monotonically with increasing the wavevector transfer. For H odd, two distinct families of peaks were observed. The peaks in the first family occurred at the same

positions in ξ as for H even and had comparable intensities except that in this case the intensity of peaks decreased much faster with increasing ξ. The peaks in the second family were displaced symmetrically oppositely from the half-odd-integer values of ξ as compared with the peaks in the first family and had a much lower intensity, but which increased with increasing position along the b^*-axis.

The characteristic double-peak structure observed for H odd is presented in figure 4(a) which shows a scan along $[3, \xi, 0]$ with two well defined peaks centred at $(3, 0.474 \pm 0.002, 0)$ and $(3, 0.528 \pm 0.0002, 0)$. The single-peak structure observed for H even is illustrated in figure 4(b) which presents a long scan along $[2, \xi, 0]$ showing a magnetic peak at $(2, 0.528 \pm 0.0002, 0)$.

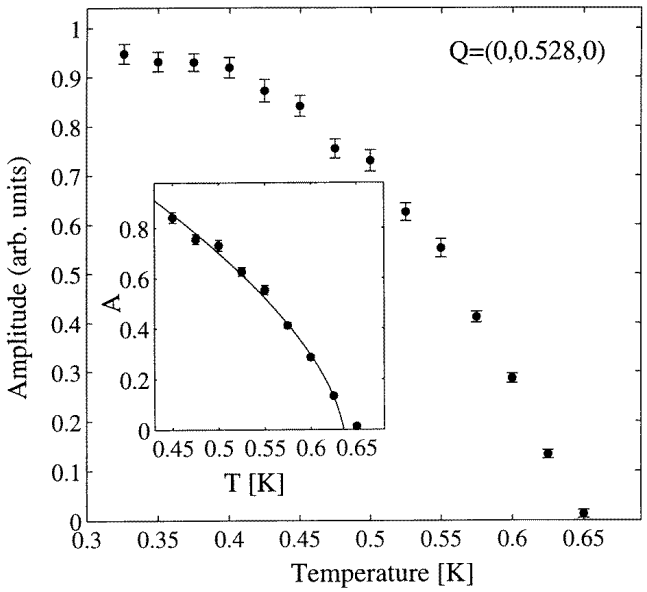

Figure 5. Intensity of the (0, 0.528, 0) magnetic reflection as a function of temperature. Inset: the solid curve is a fit to a power-law behaviour as described in the text.

The periodic arrangement of magnetic moments in the ordered phase gives rise to extra peaks in the scattering intensity at satellite positions around reciprocal-lattice points at $\boldsymbol{Q} = (H, K, L) \pm \boldsymbol{q}$ (denoted as $(H, K, L)^{\pm}$), where $\boldsymbol{q}$ defines the periodicity of the magnetic structure. The positions of the observed magnetic reflections show that the spin ordering is modulated along the b-axis, i.e. the direction of the magnetic chains. A single value of the ordering wavevector $\boldsymbol{q} = (0, 0.472, 0)$ (rlu) is sufficient to account for all measured peaks. This suggests that the magnetic structure is a single-$\boldsymbol{q}$ incommensurate modulation propagating along the b-axis.

Scans through the $(010)^-$ magnetic reflection with increasing temperature showed that the ordering wavevector is within error independent of temperature and that the intensity decreases as the temperature approaches the Néel point $T_N = 0.62 \pm 0.01$ K, as shown in figure 5. The inset of the figure shows a fit (solid line) of the $(010)^-$ magnetic peak intensity to a power-law behaviour $I \propto (T_N - T)^{2\beta}$, where β is the critical exponent associated with the order parameter. The fit gives a value of the exponent of $\beta = 0.31 \pm 0.025$.

4. Theoretical analysis

4.1. Group theory analysis of possible magnetic structures

In this section the magnetic structures compatible with the symmetry of the crystal are determined. There are four independent Cu spins in the unit cell and each spin belongs to a different magnetic sublattice. With each spin having three components in the x-, y- and z-directions, the magnetic structure is determined by giving the 12 spin components of the spins in each unit cell. The 12 components form a representation for the magnetic structure and group theory can be used to reduce this representation to its irreducible representations, as described for example in [11].

Let $\boldsymbol{m}_{\boldsymbol{k},j}$ be the Fourier components of the magnetic moment distribution, where j is the magnetic sublattice. Since the crystal structure has inversion symmetry and the moment distribution must be real, $\boldsymbol{m}_{-\boldsymbol{k},j} = \boldsymbol{m}^*_{\boldsymbol{k},j}$. Only magnetic satellites with $\boldsymbol{q} = (0, 0.472, 0)$ (rlu) were observed, so these are the only Fourier components that will be considered. The magnetic moment in unit cell l and on sublattice j is then given by

$$\boldsymbol{m}_{l,j} = \boldsymbol{m}_{\boldsymbol{q},j}\mathrm{e}^{-\mathrm{i}\boldsymbol{q}\cdot\boldsymbol{r}_l} + \boldsymbol{m}_{-\boldsymbol{q},j}\mathrm{e}^{\mathrm{i}\boldsymbol{q}\cdot\boldsymbol{r}_l} = 2|\boldsymbol{m}_{\boldsymbol{q},j}|\cos(\boldsymbol{q}\cdot\boldsymbol{r}_l + \varphi_{\boldsymbol{q},j}) \tag{1}$$

where $\boldsymbol{r}_l$ defines the position of the unit cell (expressed in units of the direct lattice) and $\varphi_{\boldsymbol{q},j}$ is a phase associated with sublattice j.

The wavevector $\boldsymbol{q}$ describing the periodicity of the magnetic structure in the ordered phase has an associated space group $\mathrm{G}_{\boldsymbol{q}}$ that depends on the symmetry of the underlying crystal structure. According to Landau's theory of continuous phase transitions [11], the order parameter of the transition is a linear combination of the basis vectors belonging to one and the same irreducible representation $\Gamma_{\boldsymbol{q}\nu}$ of the space group $\mathrm{G}_{\boldsymbol{q}}$. For a magnetic phase transition the basis vectors are formed from the spin components on the different sublattices, and the vectors that can coexist belong to the same irreducible representation.

Table 1. Irreducible representations of the space group $\mathrm{G}_{\boldsymbol{q}}$ for $\boldsymbol{q} = (0, q, 0)$, where $\beta = \mathrm{e}^{-\mathrm{i}\pi q}$.

$\mathrm{G}_{\boldsymbol{q}}$	e	2_{1y}	a	n	Basis vectors
Γ_1	1	β	1	β	A_x, G_y, C_z
Γ_2	1	$-\beta$	1	$-\beta$	G_x, A_y, F_z
Γ_3	1	β	-1	$-\beta$	C_x, F_y, A_z
Γ_4	1	$-\beta$	-1	β	F_x, C_y, G_z

The irreducible representations of $\mathrm{G}_{\boldsymbol{q}}$ are obtained from the point group of the *Pnma* space group, $\mathrm{D}_{2\mathrm{h}} = \{e, 2_x, 2_y, 2_z, \bar{1}, m_x, m_y, m_z\}$, where x, y and z are along the crystallographic a-, b- and c-axes, respectively. The symmetry elements that leave the ordering wavevector $\boldsymbol{q} = (0, q, 0)$ invariant are the little group $\mathrm{g}_{\boldsymbol{q}} = \{e, 2_y, m_x, m_z\} = C_{2\mathrm{v}}$. In the *Pnma* space group the point rotation 2_y is the twofold screw axis $2_{1y}(\frac{1}{2}, y, 0)$, the mirror plane m_x is the diagonal glide plane $\boldsymbol{n} \perp [100]$ with glide vector $\frac{1}{2}(\boldsymbol{b} + \boldsymbol{c})$ and the mirror plane m_z is the axial glide plane $\boldsymbol{a} \perp [001]$ with a glide vector $\frac{1}{2}\boldsymbol{a}$, as shown in figure 6(a). The space group of the wavevector $\boldsymbol{q}$ is then $\mathrm{G}_{\boldsymbol{q}} = \{e, 2_{1y}, n, a\}$. It contains the elements of $\mathrm{g}_{\boldsymbol{q}}$ with the associated translations $\boldsymbol{t}_i$ that make them symmetry elements of the *Pnma* space group. Table 1 gives the irreducible representations of $\mathrm{G}_{\boldsymbol{q}}$ as $\Gamma_{\boldsymbol{q}\nu}(\{\omega_i|\boldsymbol{t}_i\}) = \gamma_{\boldsymbol{q}\nu}(\omega_i)\mathrm{e}^{-\mathrm{i}\boldsymbol{q}\cdot\boldsymbol{t}_i}$, where the $\gamma_{\boldsymbol{q}\nu}$ are the characters of $\mathrm{g}_{\boldsymbol{q}}$ [12]. The four possible basis vectors for the magnetic moments in the four sublattices are given by the column

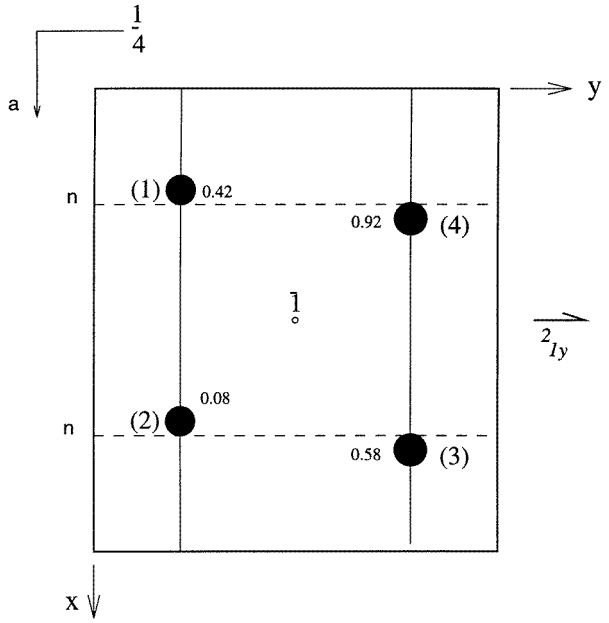

(a)

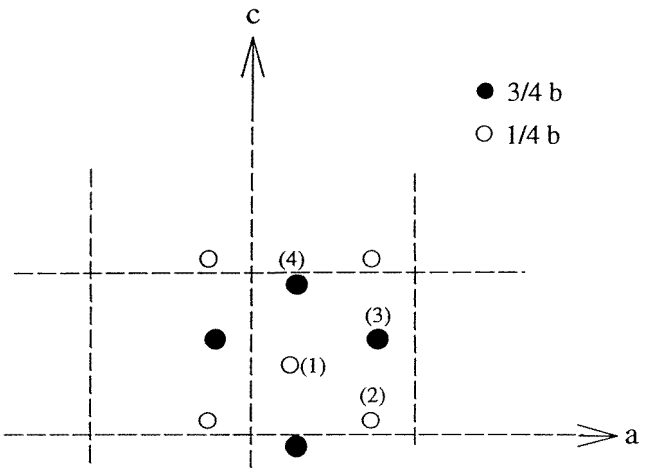

(b)

Figure 6. (a) Projection of the magnetic atoms on the (a, b) plane showing the symmetry elements that make up the space group $G_{\boldsymbol{q}} = \{e, 2_{1y}, n, a\}$. The height in z is shown next to each atom. (b) Projection of the magnetic atoms on the (a, c) plane.

vectors

$$\boldsymbol{F} = \begin{bmatrix} 1 \\ 1 \\ \beta \\ \beta \end{bmatrix} \qquad \boldsymbol{C} = \begin{bmatrix} 1 \\ 1 \\ -\beta \\ -\beta \end{bmatrix} \qquad \boldsymbol{G} = \begin{bmatrix} 1 \\ -1 \\ \beta \\ -\beta \end{bmatrix} \qquad \boldsymbol{A} = \begin{bmatrix} 1 \\ -1 \\ -\beta \\ \beta \end{bmatrix} \tag{2}$$

where $\beta = e^{-i\pi q}$ is a phase factor that occurs because sublattices (3) and (4) are displaced along the propagation direction by $\boldsymbol{b}/2$ with respect to sublattices (1) and (2). For example if the structure corresponds to an F mode the following relations hold:

$$\boldsymbol{m}_{\boldsymbol{q},2} = \boldsymbol{m}_{\boldsymbol{q},1} \qquad \boldsymbol{m}_{\boldsymbol{q},3} = e^{-i\pi q}\boldsymbol{m}_{\boldsymbol{q},1} \qquad \boldsymbol{m}_{\boldsymbol{q},4} = e^{-i\pi q}\boldsymbol{m}_{\boldsymbol{q},1}. \tag{3}$$

In this structure the spins in sublattices (1) and (2) are parallel and so are the spins in sublattices (3) and (4), but there is a difference of πq between the phases of the spins in the two pairs of sublattices.

The magnetic structure factor is given by

$$\boldsymbol{F}_M(\boldsymbol{Q}) = \sum_{j=1}^{4} \boldsymbol{m}_{\boldsymbol{q},j} e^{i\boldsymbol{Q}\cdot\boldsymbol{r}_j} \tag{4}$$

where $\boldsymbol{Q} = (H, K+q, L)$ is the wavevector of the magnetic superlattice peak and $\boldsymbol{r}_j$ is the position of spin j in the unit cell (expressed in units of the direct lattice). For reflections in the (a, b) plane and for a spin structure corresponding to basis vector $\boldsymbol{F}$, the magnetic structure factor is

$$\boldsymbol{F}_M^{(F)}(Q) = 4\boldsymbol{m}_{\boldsymbol{q},1}\delta_{H,2p}(\cos(2\pi Hx)\delta_{K,2s} + i\sin(2\pi Hx)\delta_{K,2s+1}) \tag{5}$$

and similar expressions can be obtained for the other modes. Here δ is the Kronecker symbol and p and s are integers. Since $x = 0.23 \approx 1/4$ this spin structure gives strong reflections for $H = 2p$, $K = 2s$ only. Similarly, every other mode gives strong reflections only in certain Brillouin zones: G (when $H = 2p+1$, $K = 2s+1$), C (when $H = 2p$, $K = 2s+1$) and A (when $H = 2p+1$, $K = 2s$). Figure 3 summarizes these results.

4.2. Exchange interactions and ground-state energy

The energy and the stability of possible spin configurations modulated along the chain direction have been studied using a mean-field approximation [14]. The ground-state energy has been calculated for the isotropic Heisenberg exchange Hamiltonian $H = \sum_{\boldsymbol{r},\boldsymbol{r}'} J_{\boldsymbol{r},\boldsymbol{r}'}\boldsymbol{S}_{\boldsymbol{r}} \cdot \boldsymbol{S}_{\boldsymbol{r}'}$, where $J_{\boldsymbol{r},\boldsymbol{r}'}$ is the exchange interaction between spins at $\boldsymbol{r}$ and $\boldsymbol{r}'$, and the interaction is restricted to nearest neighbours only. In the mean-field approximation every spin in sublattice i satisfies

$$\lambda\boldsymbol{S}_{\boldsymbol{r}_{l,i}} = \sum_{j=1}^{4}\sum_{l'} J_{\boldsymbol{r}_{l,i},\boldsymbol{r}_{l',j}}\boldsymbol{S}_{\boldsymbol{r}_{l',j}} \tag{6}$$

where $\boldsymbol{r}_{l,i}$ indexes an atom in unit cell $\boldsymbol{l}$ and on sublattice i. Fourier transformation of equation (6) gives the eigenvalue equation

$$(\boldsymbol{\eta} - \lambda\mathbf{l})\boldsymbol{m}_{\boldsymbol{k}} = 0 \tag{7}$$

where $\boldsymbol{\eta}$ is a 4×4 matrix with elements $\eta_{ij} = \sum_l J_{\boldsymbol{r}_{0,i},\boldsymbol{r}_{l,j}} e^{i\boldsymbol{q}\cdot(\boldsymbol{r}_{0,j}-\boldsymbol{r}_{l,j})}$ the interaction between sublattices i and j. The column vectors $\boldsymbol{m}_{\boldsymbol{q},j} = \sum_l \boldsymbol{S}_{\boldsymbol{r}_{l,j}} e^{i\boldsymbol{q}\cdot(\boldsymbol{r}_{l,j}-\boldsymbol{r}_{0,j})}$ are the eigenvectors of the spin configuration and $\mathbf{l}$ is the 4×4 identity matrix. The origin of magnetic sublattice i is at atom $\boldsymbol{r}_{\mathbf{0},i}$ and $\boldsymbol{q} = (0, q, 0)$ is the ordering wavevector of the magnetic structure.

The interaction matrix $\boldsymbol{\eta}$ is given by

$$\boldsymbol{\eta} = \begin{pmatrix} \varepsilon_{11} & \varepsilon_{12} & \varepsilon_{13}\beta^* & \varepsilon_{14}\beta^* \\ \varepsilon_{12} & \varepsilon_{11} & \varepsilon_{14}\beta^* & \varepsilon_{13}\beta^* \\ \varepsilon_{13}\beta & \varepsilon_{14}\beta & \varepsilon_{11} & \varepsilon_{12} \\ \varepsilon_{14}\beta & \varepsilon_{13}\beta & \varepsilon_{12} & \varepsilon_{11} \end{pmatrix} \tag{8}$$

where $\varepsilon_{11} = 2J_{11}\cos 2\pi q$, $\varepsilon_{12} = 4J_{12}$, $\varepsilon_{13} = 4J_{13}\cos \pi q$, $\varepsilon_{14} = 4J_{14}\cos \pi q$ and $\beta = \mathrm{e}^{-\mathrm{i}\pi q}$. Every spin has two neighbours on its own sublattice and four neighbours on each of the other three sublattices, as shown in figure 6(b). For example a spin on sublattice (1) interacts with two nonequivalent pairs of spins on sublattice (2) and since all spins lie in the same b-plane the term η_{12} is the sum of the four interactions with no additional phase factor. There is no loss in the generality of the problem on defining J_{12} as the average interaction between a spin on sublattice (1) and its two types of nonequivalent neighbour on sublattice (2), so that $\eta_{12} = 4J_{12}$. Similarly, J_{13} is the average interaction between one spin on sublattice (1) and its two types of nonequivalent neighbour on sublattice (3), whereas J_{14} is the interaction between one spin on sublattice (1) and its four equivalent neighbours on sublattice (4). The exchange interaction between spins on the same sublattice is denoted by J_{11}. The solutions of the eigenvalue equation (7) are the basis vectors given in equation (2) with the wavevector-dependent eigenvalues

$$\begin{aligned}
\lambda_F &= \varepsilon_{11} + \varepsilon_{12} + \varepsilon_{13} + \varepsilon_{14} \\
\lambda_C &= \varepsilon_{11} + \varepsilon_{12} - \varepsilon_{13} - \varepsilon_{14} \\
\lambda_G &= \varepsilon_{11} - \varepsilon_{12} + \varepsilon_{13} - \varepsilon_{14} \\
\lambda_A &= \varepsilon_{11} - \varepsilon_{12} - \varepsilon_{13} + \varepsilon_{14}.
\end{aligned} \tag{9}$$

The total energy for a spin structure corresponding to basis vector $\boldsymbol{F}$ is $E_F = 2N\lambda_F M^2$, where M is the magnitude of the ordered moment and N is the number of unit cells in the crystal. The ordering wavevectors which minimize the energy of each basis vector separately are given by

$$\begin{aligned}
\cos \pi q_F &= -\cos \pi q_C = -\frac{J_{13} + J_{14}}{2J_{11}} \\
\cos \pi q_A &= -\cos \pi q_G = \frac{J_{13} - J_{14}}{2J_{11}}
\end{aligned} \tag{10}$$

with the minimum energies for each basis vector given by

$$\begin{aligned}
\lambda_F(q = q_F) = \lambda_C(q = q_C) &= -2J_{11} + 4J_{12} - \frac{(J_{13} + J_{14})^2}{J_{11}} \\
\lambda_A(q = q_A) = \lambda_G(q = q_G) &= -2J_{11} - 4J_{12} - \frac{(J_{13} - J_{14})^2}{J_{11}}.
\end{aligned} \tag{11}$$

5. Analysis and discussion

5.1. The magnetic structure

The intensity of a magnetic reflection at $\boldsymbol{Q} = (HKL) \pm \boldsymbol{q}$ is given by [11]

$$I(Q) = cp^2 f^2(Q)|F_M^{\perp}(Q)|^2 \tag{12}$$

where $f(Q)$ is the magnetic form factor, $p = 2.7$ fm is the scattering length for a moment of $1\mu_B$, $F_M^{\perp}(Q)$ is the component of the magnetic structure factor perpendicular to the scattering wavevector and c is a proportionality constant that can be calculated from the intensity of the nuclear Bragg peaks. By comparing the observed neutron scattering (figure 3) with the expressions for the scattering from the four possible spin basis vectors, three coexisting basis vectors are identified: scattering by a vector C gives rise to the strong peaks with H even, while the scattering for the peaks with H odd arises from a basis vector G and a smaller basis vector A. All of these spin structures have the same

Table 2. Magnetic structure factors squared extracted from different measurements on the magnetic Bragg peaks as described in the text.

Mag. peak	Basis vectors	a_x	a_y	a_z	$\|F(Q)\|^2$ Peak amp.	$\|F(Q)\|^2$ Scan [010]	$\|F(Q)\|^2$ Scan [100]	$4\|M_x\|^2$	$4\|M_y\|^2$	$4\|M_z\|^2$
$(010)^-$	C_z	0	0	1	7.57	7.57	7.57	—	—	7.57
$(010)^+$	C_z	0	0	1	6.63	5.73	5.61	—	—	5.99 ± 0.45
$(030)^-$	C_z	0	0	1	5.76	8.09	4.75	—	—	6.20 ± 1.39
$(110)^-$	G_y	0.00	0.67	0	4.73	5.15	4.43	—	7.11 ± 0.44	—
$(110)^+$	G_y	0.01	0.21	0	1.04	1.11	0.74	—	4.57 ± 0.76	—
$(100)^+$	$A_x + G_y$	0.31	0.01	0	0.25	—	—	0.58	—	—
$(120)^-$	$A_x + G_y$	0.77	0.01	0	0.38	0.60	—	0.57 ± 0.14	—	—
$(210)^-$	C_z	0	0	0.93	5.48	5.76	4.89	—	—	5.77 ± 0.38
$(210)^+$	C_z	0	0	0.93	3.54	4.34	2.85	—	—	3.83 ± 0.65
$(310)^-$	$A_x + G_y$	< 0.01	0.82	0	3.97	4.13	4.24	—	5.01 ± 0.13	—
$(300)^+$	$A_x + G_y$	0.03	0.12	0	0.67	0.90	1.07	—	7.33 ± 1.36	—

modulation wavevector $\boldsymbol{q} = (0, 0.472, 0)$. Table 1 shows that there is just one irreducible representation Γ_1 compatible with the scattering from C_z, G_y and A_x basis vectors†. The spin components along the z-axis arise from a C type of spin structure, whereas the spin components along the x- and y-axes arise from basis vectors A and G, respectively.

Since the three coexisting basis vectors are associated with spins along perpendicular axes, the intensity at a magnetic reflection for unpolarized neutrons is a superposition of the intensities from each spin structure taken separately. The magnetic structure factor squared for the spin structure along the z-axis is

$$|F^{\perp}_{M_z}(Q)|^2 = 4M_z^2 a_z \tag{13}$$

where M_z is the magnitude of the ordered moment along the z-axis. Similar expressions hold for the x- and y-axes with the appropriate trigonometric factors a_x, a_y and a_z given by

$$\begin{aligned} a_x &= \delta_{H,2n+1}(\cos^2(2\pi Hx)\delta_{K,2p+1} + \sin^2(2\pi Hx)\delta_{K,2p})\sin^2\alpha_Q \\ a_y &= \delta_{H,2n+1}(\cos^2(2\pi Hx)\delta_{K,2p} + \sin^2(2\pi Hx)\delta_{K,2p+1})\cos^2\alpha_Q \\ a_z &= \delta_{H,2n}(\cos^2(2\pi Hx)\delta_{K,2p+1} + \sin^2(2\pi Hx)\delta_{K,2p}) \end{aligned} \tag{14}$$

where α_Q is the angle between $\boldsymbol{Q}$ and the [100] axis.

Table 2 presents the magnetic structure factors squared (in arbitrary units) as extracted from measurements of the magnetic peak amplitudes and integrated intensities for scans through the magnetic peaks along the (100) and (010) directions in reciprocal space. The normalization constants are chosen so that the value corresponding to the $(010)^-$ peak is the same in all three sets of measurements. The last three columns of the table give the amplitudes squared of the ordered moment along the x-, y- and z-axes obtained by comparing the magnetic structure factors for each peak, averaged over the three sets of measurements, with the predictions of equations (13) and (14). The $(100)^+$ and $(120)^-$ peaks contain contributions from both basis vectors A_x and G_y. The ordered moment along x is estimated by subtracting the contribution of the moment along y by using the intensity of the neighbouring peaks $(110)^-$ and $(110)^+$, respectively. The average values for the

† With the observation that if the ordering wavevector is defined as $\boldsymbol{q} = (0, 0.528, 0)$ then the irreducible representation is Γ_2 and the modes are F_z, A_y and G_x. The two descriptions are totally equivalent.

ordered moments estimated from intensities of different magnetic peaks are consistent to within 20%. This discrepancy is due to the intensity of peaks at large wavevectors being smaller than expected. A similar discrepancy was found in the case of nuclear peaks where the (220) reflection was 30% less intense than expected when compared with the (200) and (020) peaks which had the expected ratio of intensities.

The resulting distribution of the magnetic intensity among the three coexisting basis vectors is A_x:G_y:$C_z = 0.57 \pm 0.15$:5.18 ± 0.12:5.61 ± 0.25, which gives the moment amplitude ratio M_x:M_y:$M_z = 0.75 \pm 0.1$:2.27 ± 0.03:2.36 ± 0.05. In this spin configuration the components of the ordered magnetic moment are given by equations (1) and (2):

$$m^x_{l,j} = M_x \cos(\boldsymbol{q} \cdot \boldsymbol{r}_{l,j} + \varphi_x) \times \begin{Bmatrix} 1 & j=1 \\ -1 & j=2 \\ -1 & j=3 \\ 1 & j=4 \end{Bmatrix}$$

$$m^y_{l,j} = M_y \cos(\boldsymbol{q} \cdot \boldsymbol{r}_{l,j} + \varphi_y) \times \begin{Bmatrix} 1 & j=1 \\ -1 & j=2 \\ 1 & j=3 \\ -1 & j=4 \end{Bmatrix}$$

$$m^z_{l,j} = M_z \cos(\boldsymbol{q} \cdot \boldsymbol{r}_{l,j} + \varphi_z) \times \begin{Bmatrix} 1 & j=1 \\ 1 & j=2 \\ -1 & j=3 \\ -1 & j=4 \end{Bmatrix} \tag{15}$$

where $\boldsymbol{r}_{l,j}$ is the position of the atom in cell $\boldsymbol{l}$ and on sublattice j.

At low enough temperatures, we expect the ordered moment to attain the saturation value, and the only incommensurate structure compatible with the spins having a constant ordered amplitude is a helimagnetic ordering in which the spins may rotate on a circle within an easy plane. This structure is consistent with the calculated ratio between amplitudes of spin components ($M_z \approx M_y \gg M_x$) and is allowed by equation (15) if all three sine-wave modulations couple together so that the spins rotate in a circle situated mainly in the (b, c) plane. The small but nonzero magnetic moment along the x-direction shows that this plane of rotation is tilted towards the x-axis, so the rotation plane makes a dihedral angle $\phi = \tan^{-1}(M_x/M) = 17.7 \pm 2^\circ$ with the (b, c) plane, where M is the average of M_y and M_z. Taking into account the local symmetry at the Cu sites and the orientation of the magnetic easy axis it is probable that the plane of rotation of the spins contains the b-axis and is tilted towards the local easy axis which makes an angle $\alpha = 38^\circ$ with the c-axis [4], as shown in figure 1. The ordering is then cycloidal along the chains with spins rotating in a plane that contains the propagation direction b. The phase differences between the four independent chains in the unit cell can be determined from equation (15) and are shown schematically in figure 7(a). All of the spins in one chain have the same plane of rotation and consecutive spins make an angle $2\pi q = 169.92^\circ$, as illustrated in figure 7(b). Chains (1) and (3), which are related by inversion symmetry, have parallel easy planes, but the rotation of the spins occurs in opposite directions. This easy plane is obtained from the (b, c) plane by rotation around the b-axis with an angle ϕ in the anti-clockwise direction. The same is true for chains (2) and (4), the only difference being that their easy plane is obtained from the (b, c) plane by rotation around the b-axis with an angle ϕ in the clockwise direction. This spin ordering is obtained from equation (15) if $\varphi_x = (\pi/2)$, $\varphi_y = 0$ and $\varphi_z = -(\pi/2)$.

The absolute magnitude of the ordered magnetic moment was estimated by comparing the intensity of each magnetic peak with the intensity of the closest nuclear peak, the value for the latter being given by $I_{(HKL)} = c|G_{(HKL)}|^2$ where c is the same proportionality

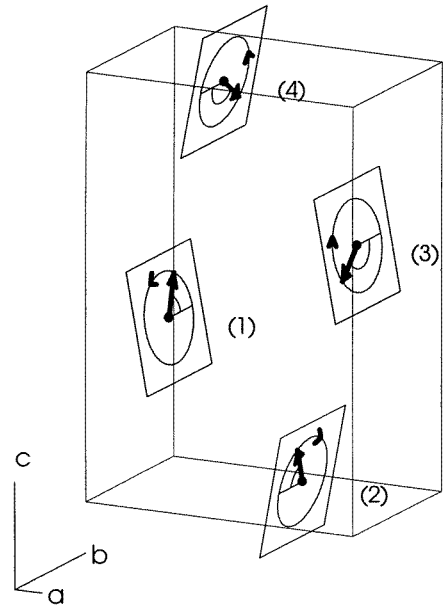

(a)

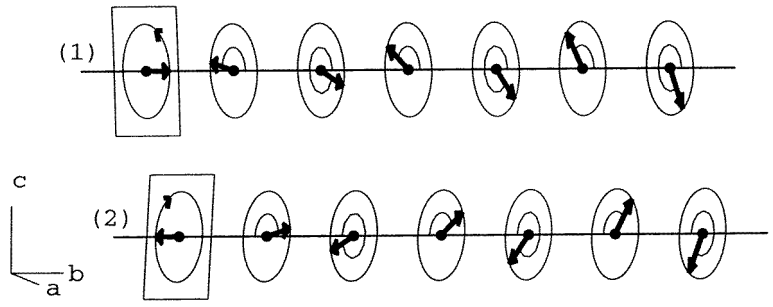

(b)

Figure 7. (a) A schematic diagram of the easy planes and sense of rotation for the spins in the four magnetic chains in the unit cell of Cs_2CuCl_4. (b) A diagram of the parallel chains (1) and (2) showing the cycloidal spin ordering propagating along the chains. Notice the opposite sense of rotation of the spins in the two chains and the fact that the z-components are always parallel whereas the x- and y-components are antiparallel. This is a consequence of the superposition of spin structures of type C_z, G_y and A_x.

constant as in equation (12) and $G_{(HKL)}$ is the nuclear structure factor. Comparison was made between values of the peak amplitudes and integrated intensities for scans through the Bragg points in the [100] and [010] directions in reciprocal space and angular scans ω and $(\theta, 2\theta)$. The nuclear peaks used for reference were the (020), (200) and (220) Bragg reflections. The resulting amplitudes of the ordered magnetic moment at $T = 0.3$ K are $M_x = (0.24 \pm 0.02)\mu_B$, $M_y = (0.78 \pm 0.02)\mu_B$ and $M_z = (0.84 \pm 0.04)\mu_B$. Room temperature ESR measurements of the g-factor [13] gave for the saturation value of the magnetic moment $M = g\mu_B S$ the values $M_x = 1.10\mu_B$, $M_y = 1.04\mu_B$ and $M_z = 1.15\mu_B$.

Our measurements show that there is a reduction $\Delta S/S = (25 \pm 2)\%$ in the amplitude of the ordered spin along the main ordering directions y and z, which may be due to quantum fluctuations. The excitations in the ordered phase and the zero-point spin reduction will be considered in a forthcoming paper.

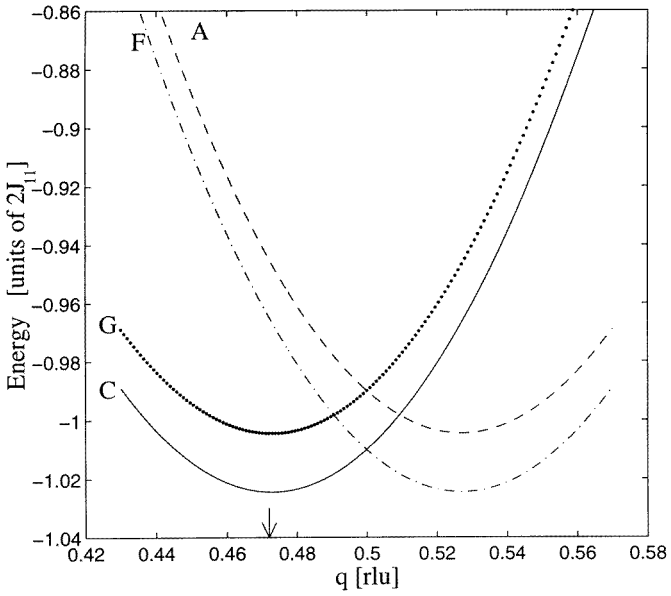

Figure 8. Behaviour of the threefold-degenerate energy levels of the four basis vectors F, C, G and A of the isotropic exchange Hamiltonian with respect to the modulation wavevector. The arrow indicates the measured value of the ordering wavevector q.

5.2. Magnetic energy levels for the isotropic system

This section compares the magnetic energy levels of different spin configurations and analyses the conditions in which the observed magnetic structure is the most stable one. The interaction Hamiltonian considered is the isotropic Heisenberg exchange. The effects of a small magnetic anisotropy are postponed until the next section.

In the theoretical analysis in section 4 it was shown that any allowed magnetic structure in Cs_2CuCl_4 consists of a superposition of basis vectors belonging to one of the irreducible representations Γ of the space group $G_{\boldsymbol{q}}$ and the results show that the ordering is associated with Γ_1. In the absence of any anisotropy a mean-field calculation gives four triply degenerate energy levels corresponding to the four types of basis vector F, C, G and A, as shown in equation (9). The degeneracy is a consequence of equal energies for the ordering with spins along the x-, y- and z-axes. Each of these energy levels has a dispersion versus ordering wavevector $\boldsymbol{q}$ and, for small values of the interchain exchanges, has a minimum at $\boldsymbol{q}$ close to the zone boundary of the crystallographic unit cell along the b^* direction, as derived in equation (10). Since the observed magnetic structure consists of strong vectors C and G with an ordering wavevector $\boldsymbol{q} = 0.472$ (rlu), this suggests that both structures are stable at that $\boldsymbol{q}$ and have only a small energy difference. A possible behaviour for the energy levels in this case is shown in figure 8. In the following we shall concentrate only

on q-values in the first Brillouin zone ($q < 0.5$) since values of q on the other side of the zone boundary provide an equivalent description, as explained earlier.

Just below the transition temperature the magnetic structure is a sine wave associated with the basis vector with the lowest energy level and the ordering wavevector corresponds to the minimum in the dispersion of this level. On decreasing the temperature below T_N the amplitude of the ordered moment increases and the incommensurate single-sine-wave ordering becomes unstable because it predicts that at certain sites the total ordered moment is zero. A more stable structure is a helimagnetic ordering in which the ordered moment has a constant value on every site and the spin rotates in a plane. This ordering is then given by a superposition of at least two sine waves and the ordering wavevector is at an intermediate value between the most stable qs of the constituent sine waves. On decreasing the temperature below T_N there is a gradual transition between these two types of incommensurate structure with a corresponding change in wavevector. Measurements on Cs_2CuCl_4 show that the ordering wavevector is, within error, independent of temperature for 0.3 K $\leqslant T \leqslant T_N$, which suggests that both basis vectors C and G have energy minima at very close values of q, and in this case equation (10) gives $J_{13} \approx 0$ and $J_{14}/J_{11} = 17\%$. The energy gap between the two levels is $\lambda_G - \lambda_C = -8J_{12}$, with level C being the lowest if $J_{12} < 0$ (ferromagnetic) and the two levels overlapping for $J_{12} = 0$. The energies in figure 8 are obtained from equation (9) if $J_{13} = 0$, $J_{14}/J_{11} = 17\%$ and $J_{12}/J_{11} = -0.5\%$.

5.3. Magnetic anisotropy. Crystal-field effects

In the following we shall study the origins of magnetic anisotropy and its effects on the energy of different spin configurations. The free Cu^{2+} ion has a $3d^9$ ($L = 2$) fivefold-degenerate orbital ground state which is split by the crystal field of the Cl^- ligand ions in Cs_2CuCl_4 [15]. The local symmetry at Cu sites is nearly tetrahedral with a small tetragonal distortion along one of the fourfold axes, the point group symmetry being D_{2d} to a good approximation [4]. The local symmetry axes are indicated by dashed lines in figure 1 for each of the four Cu atoms in the unit cell. In the given crystal-field environment the orbital ground state is a singlet $|2^a\rangle = (1/\sqrt{2})(|+2\rangle - |-2\rangle)$, where $|M_L\rangle$ is an eigenstate of the orbital angular momentum and the quantization direction is along the local symmetry axis. Taking the spin degeneracy into account the ground state becomes a doublet $|2^a, \pm\rangle$, where the first label denotes the orbital state and the second the spin state. Through the spin–orbit coupling higher orbital states are mixed into the ground state [16], which in a first-order approximation has the wavefunctions

$$|+\rangle = |2^a, +\rangle - \frac{\lambda}{\Delta_1}|2^s, +\rangle + \frac{\lambda}{\sqrt{2}\Delta_0}|-1, -\rangle$$
$$|-\rangle = |2^a, -\rangle + \frac{\lambda}{\Delta_1}|2^s, -\rangle - \frac{\lambda}{\sqrt{2}\Delta_0}|+1, +\rangle$$

where $\lambda = -828$ cm^{-1} is the spin–orbit coupling in the free ion, and $\Delta_0 = 4800$ cm^{-1} and $\Delta_1 = 7900$ cm^{-1} are the energies of the higher orbital states relative to the ground state [15]. The resulting g-values are $g_{||} = 2 - 8\lambda/\Delta_1$ and $g_\perp = 2 - 2\lambda/\Delta_0$ and they qualitatively reproduce the observed uniaxial anisotropy $g_{||} > g_\perp$ [13]. An effective spin $T = \frac{1}{2}$ can be associated with the ground-state doublet with the effective spin operators being related to the real spin operators by

$$S_{x'} = \gamma T_{x'}$$
$$S_{y'} = \gamma T_{y'}$$
$$S_{z'} = \rho T_{z'}$$

where z' is the local symmetry axis, and $y' = y$ and (x', y', z') form a right-hand coordinate system. The renormalization factors ρ and γ are given by $\rho = 1 - (\lambda/\Delta_0)^2$ and $\gamma = 1 - \frac{1}{2}(\lambda/\Delta_0)^2 - 2(\lambda/\Delta_1)^2$. Since $\rho > \gamma$ this leads to anisotropy in the exchange interactions, the easy axis for the spins being the local symmetry axis z', indicated for each spin in the unit cell in figure 1.

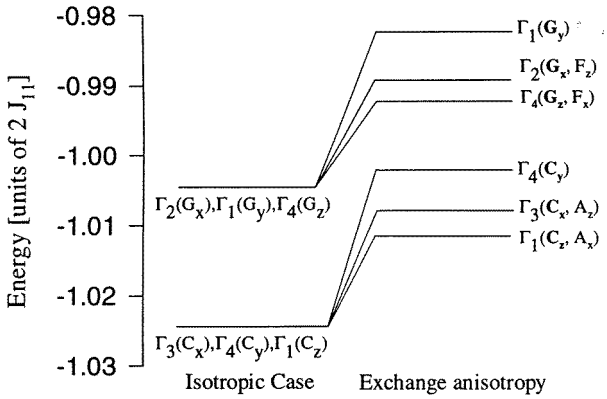

Figure 9. The splitting of the low-lying energy levels for $q = 0.472$ (rlu) in the presence of anisotropy.

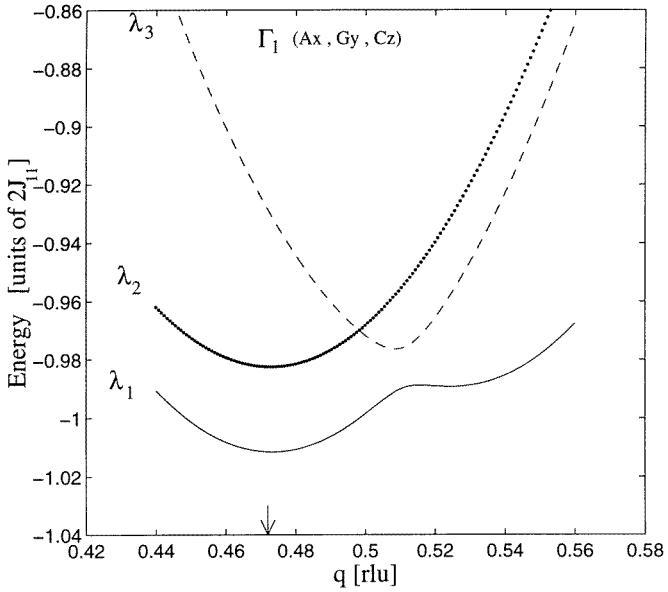

Figure 10. Behaviour of the energy levels of the irreducible representation Γ_1 in the presence of exchange anisotropy. The measured value of the ordering wavevector is indicated by a vertical arrow.

By transforming from the local coordinate system for each of the four Cu atoms to the crystallographic axes, the exchange Hamiltonian can be expressed in terms of the effective

spins along the x-, y- and z-axes. A mean-field theory calculation of the magnetic ground-state energy following the lines of section 4.2 shows that the overall effect of anisotropy is the splitting of the threefold-degenerate energy levels obtained in the isotropic case. The basis vectors F_y, C_y, G_y and A_y along y are still eigenvectors of the anisotropic exchange Hamiltonian, but with the energy levels renormalized by an overall factor γ^2. The anisotropy in the exchange interaction couples basis vectors along x and z, but since the anisotropy has the symmetry of the space group, only basis vectors belonging to the same irreducible representation Γ are coupled together, i.e. C_z and A_x in Γ_1. Figure 9 shows the low-lying energy levels for $q = 0.472$ (rlu) in the presence of anisotropy and for the same values of the interchain exchange interactions as in figure 8. All levels are shifted upwards in energy because both renormalization constants ρ and $\gamma < 1$. For a given basis vector, the energy of the spin configuration with spins along z is lowest since the z-axis is closest to the easy axes of the spins, and the energy of the spin configuration with spins along y is highest because the y-axis is a hard axis for all of the spins. The overall lowest energy level is $\Gamma_1(\boldsymbol{C}_z, A_x)$ which denotes a basis vector of the Γ_1 irreducible representation which consists of mainly the vector C_z with a small admixture of A_x. Figure 10 shows the behaviour of the resulting energy levels of the Γ_1 irreducible representation in the presence of anisotropy and for the same interchain exchange interactions as in figure 8, where the basis vectors are $|\lambda_1\rangle = b_1C_z + b_2A_x$, $|\lambda_2\rangle = G_y$ and $|\lambda_3\rangle = -b_2C_z + b_1A_x$ with q-dependent values of the coefficients b_1 and b_2. At $q = 0.472$ the coefficients are $b_1 = 0.996$ and $b_2 = -0.081$ and in Γ_1 the lowest energy level is C_z with a small admixture of A_x, followed by G_y and then A_x with a small admixture of C_z. The magnetic structure predicted by figures 9 and 10 is a transverse sine wave with basis vector $\Gamma_1(\boldsymbol{C}_z, A_x)$ just below T_N and a helimagnetic ordering with a superposition of states $\Gamma_1(\boldsymbol{C}_z, A_x)$ and G_y at low temperatures. This result agrees with the observed structure at low temperatures consisting of strong vectors C_z and G_y with a less intense vector A_x. The negative sign of b_2/b_1 suggests that there is a phase difference of π between the phases of the spin orderings along x and z which results in a tilt of the plane of rotation of the spins from the (b, c) plane towards the local easy axis for each chain, which is consistent with the structure drawn in figure 7(a). An arbitrary small value of $J_{12} = -0.5\%J_{11}$ was used throughout the calculations. The reason for choosing $J_{12} < 0$ is that otherwise level G would be lower in energy than C in figure 8 and the basis vector with the lowest energy would be $\Gamma_4(\boldsymbol{G}_z, F_x)$, leading to a magnetic structure totally different to the one observed. Also, the comparable values of the observed amplitudes of the vectors C and G in the magnetic structure suggest that the energy gap between them $\lambda_G - \lambda_C = -8J_{12}$ is relatively small.

The admixing ratio of A_x into C_z can be estimated from measurements of the ordered moments ratio M_x/M_z and a direct comparison with the theoretical prediction shows that the present formalism underestimates the admixing ratio. This may be due to the fact that effects such as mixing of p states into the orbital ground state of the Cu^{2+} ion and covalency from the Cl^- ligand ions were neglected. These effects were shown to contribute to the magnetic anisotropy and to allow for the correct g-values to be obtained [15]. The admixing ratio of A_x into C_z depends strongly on anisotropy and increases with increasing anisotropy factor ρ/γ.

In a search for another mechanism that would lead to a splitting of the threefold-degenerate energy levels of the isotropic exchange Hamiltonian and thus distinguish between spin orderings along the x-, y- and z-axes, we have calculated the dipolar energy of different spin configurations. The dipolar magnetic field on each site was computed numerically by summing contributions from ferromagnetically aligned spins situated on successive planes perpendicular to the b-axis, allowing for the modulation phase factor, as described in [6].

The resulting splittings in the level C, for example, are of the order of 10^{-3} meV and predict that the levels in order of increasing energy are C_x, C_z and C_y. This result is to be compared with the splittings due to effective spin anisotropy which are of the order of 10^{-2} meV and predict the succession of energy levels $\Gamma_1(\boldsymbol{C}_z, A_x)$, $\Gamma_3(\boldsymbol{C}_x, A_z)$ and C_y, as shown in figure 9. This comparison shows that although the dipolar interaction distinguishes between basis vectors along x, y and z, the energy difference is one order of magnitude smaller than the energy difference predicted by the effective spin anisotropy and that the energy levels cannot explain the observed magnetic structure.

6. Conclusions

The magnetic structure of Cs_2CuCl_4 has been studied by elastic neutron scattering using three-axis techniques. The magnetic ordering is incommensurate along the crystallographic b-direction which coincides with the direction of main exchange interaction between spins. Results and analysis show that the structure is cycloidal with spins rotating in a plane that contains the b-axis, with two different planes of rotation in the unit cell. The incommensurate ordering was shown to be the consequence of frustration induced by the interaction between spins in chains having atoms displaced by $\boldsymbol{b}/2$. The observed magnetic structure was shown to belong to the irreducible representation Γ_1 of the space group $G_{\boldsymbol{q}}$ of the ordering wavevector. A mean-field calculation including effective spin anisotropy was used to find the conditions in which the observed spin configuration has the lowest energy of all of the magnetic structures allowed by symmetry. Dipolar energy effects were also considered, but found to be insignificant. Approximate values for the interchain exchanges that are consistent with the observed features of the magnetic structure have been proposed. We have been unable to find an explanation for the difference in the interchain exchange values based on simple superexchange arguments.

Acknowledgments

We acknowledge the financial support for the experiments from the LIP programme at Risø National Laboratory and from the EPSRC at the Institut Laue–Langevin and Oxford. The technical support offered by Moritz Lund, Jean-Louis Ragazzoni and Alan Brochier is gratefully acknowledged. Also thanks to Drs Uli Wildgruber and John Axe for assisting in the lining up of the crystal at Brookhaven and to Dr Wieslawa Sikora for providing a computer programme to check the group theory calculations. RC is very grateful to the University of Oxford for the award of a Scatcherd scholarship.

References

[1] Duxbury P M, Oitmaa J, Barber M N, van der Bilt A, Joung K O and Carlin R L 1981 *Phys. Rev.* B **24** 5149
[2] Algra H A, de Jongh L J, Blöte H W J, Huiskamp W J and Carlin R L 1976 *Physica* B **82** 239
[3] Yoshizawa H, Shirane G, Shiba H and Hirakawa K 1983 *Phys. Rev.* B **28** 3904
[4] Bailleul S, Svornos D, Porcher P and Tomas A 1991 *C. R. Acad. Sci., Paris* I **313** 1149
[5] Carlin R L, Burriel R, Palacio F, Carlin R A, Keij S F and Carnegie D W Jr 1985 *J. Appl. Phys.* **57** 3351
[6] Yoshimori A 1959 *J. Phys. Soc. Japan* **14** 807
[7] Soboleva L V, Belaev L M, Ogadzhanova V V and Vasileva M G 1981 *Krystallografiya* **26** 817
[8] Cowley R A and Bates S 1988 *J. Phys. C: Solid State Phys.* **21** 4113
[9] Longmore A, Boothroyd A T, Chen Changkang, Hu Yongle, Nutley M P, Andersen N H, Casalta H, Schleger P and Christensen A N 1996 *Phys. Rev.* B **53** 9382
[10] *International Tables for Crystallography* 1995 vol C, ed A J C Wilson (Dordrecht: Kluwer) p 391

[11] Rossat-Mignod J 1987 *Methods of Experimental Physics* vol 23, Part C, ed K Sköld and D L Price (New York: Academic) pp 79, 110
[12] Hammermesh M 1962 *Group Theory and its Applications to Physical Problems* (London: Addison-Wesley) p 125
[13] Bailleul S, Hölsä J and Porcher P 1994 *Eur. J. Solid State Inorg. Chem.* **31** 431
[14] Bertaut E F 1974 *J. Physique* **35** 659
[15] Sharnoff M 1965 *J. Chem. Phys.* **42** 3383
[16] Abragam A and Bleaney B 1970 *Electron Paramagnetic Resonance of Transition Ions* (New York: Dover) p 467